Critical aspects of membrane-free aqueous battery based on two immiscible neutral electrolytes

Paula Navalpotro [a,1], Carlos Trujillo [a,c], Iciar Montes [a], Catarina M.S.S. Neves [b], Jesus Palma [a], Mara G. Freire [b], João A.P. Coutinho [b], Rebeca Marcilla [a,*]

[a] Electrochemical Processes Unit, IMDEA Energy Institute, Avda. Ramón de La Sagra 3, 28935, Móstoles, Spain
[b] CICECO - Aveiro Institute of Materials, Chemistry Department, University of Aveiro, 3810-193, Aveiro, Portugal
[c] Faculty of Chemical Science and Technology, University of Castilla-La Mancha, Avda. Camilo José Cela 10, 13071, Ciudad Real, Spain

ARTICLE INFO

ABSTRACT

Redox Flow Batteries (RFB) stand out as a promising energy storage technology to mitigate the irregular energy generation from renewable sources. However, some hurdles limit their massive implementation including high cost of vanadium and the poor-performance of ion-selective membranes. Recently, we presented a revolutionary Membrane-Free Battery based on organic aqueous/nonaqueous immiscible electrolytes that eludes both separators and vanadium compounds. Here, we demonstrate the feasible application of this archetype in Aqueous Biphasic Systems (ABS) acting as an unprecedented Total Aqueous Membrane-Free Battery. After evaluating several organic molecules, methylviologen (MV) and 2,2,6,6-Tetramethyl-1-piperidinyloxy (TEMPO) were selected as active species due to their optimum electrochemical behavior and selective partitioning between the phases. When connected electrically, this redox-active ABS becomes a Membrane-Free Battery with an open circuit voltage (OCV) of 1.23 V, high peak power density (23 mWcm^{-2}) and excellent long-cycling performance (99.99% capacity retention over 550 cycles). Moreover, essential aspects of this technology such as the crossover, controlled here by partition coefficients, and the inherent self-discharge phenomena were addressed for the first time. These results point out the potential of this pioneering Total Aqueous Membrane-Free Battery as a new energy storage technology.

1. Introduction

An efficient use of renewable energy resources, such as solar or wind, requires mitigation or fulfilling the mismatch between its inherent intermittent energy production and the electricity demand. Energy storage can provide a safe and cost-effective solution to the irregular energy supply [1–3]. Some technical merits stand out the Redox Flow Batteries (RFBs) when compared to conventional batteries such as their scalability (~MW) and the total decoupling of energy and power [4,5]. However, one of the most important limitations that obstruct their massive penetration into the market is the high price of some of the current components of RFBs, specifically, the scarce and, in some cases also toxic, metallic compounds that are used as active species (V, Cr, etc) [6] and the poor-performing ion-exchange membranes that are necessary to avoid the electrolytes cross-mixing [7]. Different approaches have been proposed in the last years to overcome these problems. Among

them, the substitution of metallic redox species by sustainable, abundant and tunable organic redox molecules is attracting an increasing interest among the scientific community [8,9]. As a result, the number of organic molecules that are being proposed as active species for both aqueous [10–16] and nonaqueous RFBs is growing exponentially [17–22]. On the other hand, although important efforts have been made in the last decade in membrane development, significant advances have not been accomplished yet and Nafion® continues to be widespread used [23]. Besides the high cost of these membranes, they exhibit extremely poor performance in terms of conductivity and resistance in nonaqueous RFB which hugely limits their power density [24]. On account of this, the mere substitution of ion-selective membranes by inexpensive porous separators is emerging as a new trend in nonaqueous RFB. In those systems, the huge and unavoidable crossover of active species though the separator is mitigated, in some extent, by using mixed electrolytes [20]. Although it is possible to operate the battery at higher current densities, this approach

causes a large and implicit loss of material utilization because half of the active species is unusable. In an attempt to eliminate any type of membrane or separator in RFBs, classical fluidodynamic concepts have been exploited to develop membrane-less batteries using stringent flow conditions. In such batteries, the flow conditions are constrained to a laminar regime limiting the application of this concept to microfluidic devices with very low energy and power [25].

Very recently, a novel concept of Membrane-Free Battery based on the immiscibility of two electrolytes (aqueous/nonaqueous) and in which the metallic active compounds were substituted by organic redox molecules was reported. The biphasic system formed by an acidic electrolyte containing hydroquinone and N-butyl-N-methylpyrrolidinium bis(trifluoromethanesulfonyl)imide (PYR$_{14}$TFSI) ionic liquid containing para-benzoquinone constituted the first example of Membrane-Free Battery using immiscible electrolytes [26]. Furthermore, the versatility of this concept was also anticipated since it might be applied to different combinations of immiscible electrolytes containing a huge variety of redox species [27]. In fact, other groups have recently explored the Membrane-Free concept in immiscible systems containing metallic redox centers [28,29]. Although biphasic systems formed by two aqueous phases are particularly interesting in terms of sustainability, cost and environmental impact, only those based on aqueous/nonaqueous phases have been investigated for Membrane-Free batteries.

Aqueous Biphasic Systems (ABS) have been intensively studied in separation, purification and extraction processes, as an environmental friendly, low cost and scalable method in comparison with the conventional ones based on volatile organic solvents. These ABS are systems in which the addition of two water soluble compounds (two polymers [30], one polymer-one salt [31], one ionic liquid-one salt [32]) above certain concentrations causes the spontaneous separation of the system into two liquid (aqueous-rich) phases. Recently, the phase diagrams and phases compositions of novel ionic-liquid-based ABS, the partitioning coefficients of several organic redox molecules, and their electrochemical behavior in electrochemical half-cells have been reported [33]. ABS were found to be promising platforms for developing Total Aqueous Membrane-Free Batteries because the properties of each phase can be tuned by changing their composition and phase-forming components nature, giving rise to a fine control of the pH and partition coefficients of the target molecules. These properties are of paramount importance for the final application as a battery since they will determine the chemical and electrochemical stability of the redox molecules and the cross-over of active species through the interface, which will eventually affect the efficiency of the battery.

In this article, we report the first example of Total Aqueous Membrane-Free Battery using an ABS containing organic redox compounds with proper redox potentials and suitable partitioning coefficients. Specifically, we have developed different redox ABS formed by the ternary mixture of poly(ethylene glycol) with a molecular weight of 1000 g mol^{-1} (PEG$_{1000}$), sodium sulfate (Na$_2$SO$_4$) and water, in which five different organic molecules, already proposed for RFBs [12,14–16, 34–37], were dissolved. It should be noticed that, unlike our previous work related to ionic liquid-based ABS [33], the ABS used in the present work is based on PEG which is a polymer widely used in our daily products and approved by REACH. This PEG-based ABS presents several advantages such as their higher environmentally-friendly properties, lower cost and large scale production. Thus, the characterization of the ternary ABS investigated, the partition coefficients of the organic molecules and the electrochemical behavior of the two immiscible phases were determined. Finally, the most promising ABS containing 2,2,6, 6-Tetramethyl-1-piperidinyloxy (TEMPO) and Methyl Viologen (MV) was assembled and electrochemically tested as a full battery for the first time. The good electrochemical performance of this Total Aqueous Membrane-Free Battery highlights the feasibility and versatility of the Membrane-Free concept and represents an outstanding possibility for developing sustainable, low-cost and safe energy storage devices.

2. Materials and methods

2.1. Reagents

Poly(ethylene glycol) MW average 950–1050 (PEG$_{1000}$), sodium sulfate anhydrous (Na$_2$SO$_4$, ≥99%), 2,2,6,6-Tetramethyl-1-piperidinyloxy (TEMPO, 98%), Methyl Viologen dichloride hydrate (MV, 98%), anthraquinone 2-sulfonic acid sodium salt monohydrate (AQ2S, 97%), quinoxaline (QUI, 99%), and hydroquinone (H2Q, >99%) were purchased from Sigma Aldrich and used as received.

2.2. ABS characterization

The phase diagram of the ternary system composed of PEG$_{1000}$, Na$_2$SO$_4$ and water was determined by cloud-point titration method at room temperature (298 ± 1 K). To this end, aqueous solutions of Na$_2$SO$_4$ (25 wt%) and PEG$_{1000}$ (60 wt%) were prepared. This experimental procedure is based on the dropwise addition of the salt-aqueous solution into the polymer-aqueous solution until the detection of a cloudy solution (biphasic region is reached). Then water is drop-added until obtaining a transparent solution (monophasic region). This procedure was performed under stirring conditions. The phase diagrams were determined gravimetrically (±10^{-4} g).

The experimental binodal data were fitted according to the following eq [38].:

$$[Polymer] = A \exp\left[\left(B \times \ [Salt]^{0.5}\right) - \left(C \times [Salt]^3\right)\right] \tag{1}$$

where [Polymer] and [Salt] are the PEG$_{1000}$ and the Na$_2$SO$_4$ mass fraction percentages, and the parameters *A*, *B* and *C* are fitted constants.

For the determination of the tie-line, a ternary mixture composed of PEG$_{1000}$, Na$_2$SO$_4$ and H$_2$O (25, 6, 69 wt%, respectively) was gravimetrically prepared. After the complete separation of the phases, each phase was individually weighted. Then the TL was calculated by the resolution of the following 4 equation system (eqs. (2)–(5)) [38]. The compositions of the top and bottom phase are determined by the lever-arm rule.

$$[Polymer]_T = A \exp\left[\left(B \times [Salt]_T^{0.5}\right) - \left(C \times [Salt]_T^3\right)\right] \tag{2}$$

$$[Polymer]_B = A \exp\left[\left(B \times [Salt]_B^{0.5}\right) - \left(C \times [Salt]_B^3\right)\right] \tag{3}$$

$$[Polymer]_T = \frac{[Polymer]_M}{\alpha} - \frac{1-\alpha}{\alpha} \times [Polymer]_B \tag{4}$$

$$[Salt]_T = \frac{[Salt]_M}{\alpha} - \frac{1-\alpha}{\alpha} \times [Salt]_B \tag{5}$$

where *T*, *B*, and *M* designate the top phase, the bottom phase and the initial mixture, respectively. [Polymer] and [Salt] are PEG$_{1000}$ and Na$_2$SO$_4$ weight fraction. The parameter α is the ratio between the top phase weight and the total mixture weight.

2.3. Partition coefficients determination

The partition coefficient (*K*) of the active molecules (TEMPO and MV), was determined by equation (6), being an indication of the concentrations of the target species in the top to that in the bottom phases in equilibrium:

$$K = \frac{[target \ molecule]_{Top \ Phase}}{[target \ molecule]_{Bottom \ Phase}} \tag{6}$$

For determining the partition coefficients, ABS containing only one electrochemically active molecule was gravimetrically prepared, and then kept for phase separation at 298 K for at least 12 h. After phase separation, the phases were analyzed by UV spectroscopy and the

concentration of the active species in each phase determined by a previously established calibration curve.

2.4. Electrolyte formulation

For the preparation of the electrolyte an ABS composed of PEG_{1000}, Na_2SO_4 and 20 mM TEMPO-20 mM MV or 0.1 M TEMPO-0.1 M MV aqueous solution (25, 6, 69 wt %, respectively) was gravimetrically prepared. Once the phase separation was established the top phase and the bottom phase were used as catholyte and anolyte, respectively.

2.5. Electrochemical characterization of the electrolytes

The CV experiments were conducted in a Biologic VMP multichannel potentiostat at 10 mVs^{-1} and room temperature using as reference electrode Ag/AgCl and a Pt mesh as counter electrode. Ionic conductivity of the phases of the ABS was measured with Conducell 4UxF Arc sensor from Hamilton Bonaduz AG.

2.6. Assembly and electrochemical characterization of the battery

The battery was built in a glass cell by adding the same volume of each phase of the ABS (3.5 mL) and introducing one carbon felt electrode (SGL CARBON GmbH) in each one. Carbon felts (grade GFD 4.6 EA, 4.6 mm thickness) purchased from SGL CARBON GmbH were used as electrode material. In order to make them hydrophilic they were cut with rectangular shape (geometric surface area ~1.5 cm^2) and merged in 1 M NaOH solution at 80 °C during 1 h. Then they were washed up to pH = 7 with ultrapure water and dried at 100 °C overnight. The cell was galvanostatically charge-discharged on a Biologic VMP multichannel potentiostat with voltage safety limits of 1.5 and 0.7 V at current densities from C/7 to 2C. The polarization curve was obtained in a current density range of −40 to 15 mA cm^{-2} and voltage limits of 1.7 V and 0.5 V.

The capacity of the battery (C_t) was calculated by eq (7), where n is the amount of active species (mol), e$^-$ is the number of electron exchanged and F is the Faraday constant (96500 s A mol^{-1}).

$$C_t = ne^- F \tag{7}$$

Capacity utilization (%) is defined as the ratio between the discharge capacity and the theoretical capacity at one specific state of charge. It was calculated by eq (8), where SOC refers to battery state of charge and C is the discharge capacity delivered by the battery.

$$Capacity\ utilization\ \ (\%) = \frac{C}{C_t \cdot SOC} \cdot 100 \tag{8}$$

3. Results and discussion

3.1. Characterization and design of aqueous biphasic system (ABS) as suitable immiscible electrolytes

3.1.1. Phase diagram of the PEG-based ABS

Aqueous biphasic systems (ABS) are ternary mixtures composed of two solutes/phase-forming components and water that above certain concentrations, described by the respective binodal curve, undergo phase separation leading to the formation of two aqueous-rich phases, each one enriched in one of the solutes. ABS phase diagrams are usually represented in orthogonal axis, in which only the concentration of the two solutes is displayed (water composition is omitted and corresponds to the difference required to reach 100 wt%). The binodal curve of each phase diagram separates the monophasic and biphasic regions, whereas the respective tie-lines give the composition of each phase for a given initial mixture composition. In this work, one of the solutes is PEG_{1000} which is a low cost and environmentally friendly polymer that has been widely studied in ABS for extractive separation. The inorganic salt Na_2SO_4 was selected due to its high ability to form ABS and their extensive use as

supporting electrolyte. Additional advantage of the ABS formed by PEG and Na_2SO_4 is its moderate pH (5–7) that result in low corrosive character of the media, lower environmental impact in case of electrolyte leakage in the battery and high chemical and electrochemical stability of redox-active organic molecules. Fig. 1 depicts the phase diagram determined through the cloud point titration method at 25 °C and atmospheric pressure for the ABS formed by poly(ethylene glycol) (PEG_{1000}) and sodium sulfate salt (Na_2SO_4). The experimental solubility curves were correlated according to a previously proposed equation, and tie-lines determined according to a series of equations obeying the lever-arm rule and phase-forming components mass balance [38] (Table S1). The ABS was prepared with the following mixture composition: 25 wt% PEG_{1000} + 6 wt% Na_2SO_4 + 69 wt% H_2O, ensuring that the mixture point is far for the monophasic region and within the solubility range of both Na_2SO_4 and PEG. This initial mixture composition is pointed out with a red dot in Fig. 1. The composition of each phase or respective tie-line for this initial mixture composition, i.e. the composition of the PEG-rich phase (top phase) and salt-rich phase (bottom phase), is also given in Fig. 1.

3.1.2. Partition coefficients of organic molecules in the ABS

In order to behave as a battery, the ABS should contain one redox-active compound dissolved in each phase so they may act as the catholyte and anolyte. The difference between the redox potentials of the two active compounds will determine the voltage of the battery. In this Membrane-Free Battery the interface acts as a natural barrier separating catholyte and anolyte, thus should avoid the crossover of active species that would provoke the loss of efficiency. In a biphasic system, the preferential partition of each active species and cross-contamination is addressed by their respective partition coefficients (K) between the two phases. The partition coefficients (K) of several redox organic molecules in the investigated PEG-based ABS, defined as the ratio between the concentration of each redox molecule in the PEG-rich phase to that in the salt-rich phase, were determined and are shown in Fig. 2. The chemical structures and abbreviations of each redox organic molecule are also given in Fig. 2. For an efficient battery application, the partition coefficient should be as high as possible for the species separated in the top phase and as small as possible for the species separated in the bottom phase, since that ensures a high separation and low crossover. Only MV preferentially partitions to the bottom salt-rich phase of the ABS ($K \ll 1$), whereas the remaining molecules partition preferentially to the top PEG-rich phase ($K \gg 1$). This is in good agreement with the hydrophilic nature of these molecules. MV is the more hydrophilic molecule studied and
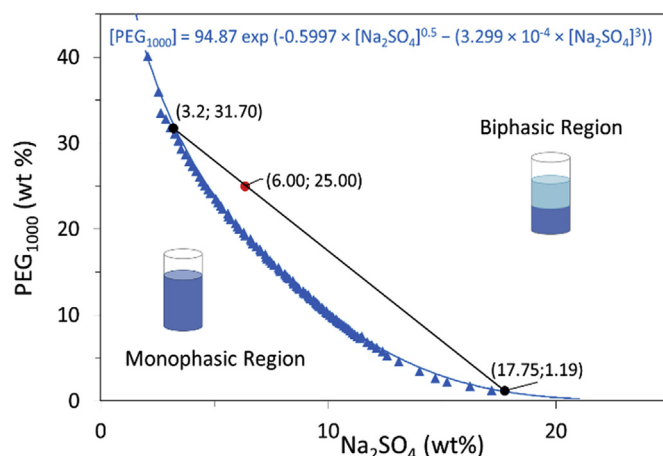

Fig. 1. Binodal curve of the phase diagram of the ABS composed of PEG_{1000} + Na_2SO_4 + H_2O (blue dots + blue line), initial mixture composition (red dot) and composition of each phase (black dots and black line representing the respective tie-line). (For interpretation of the references to colour in this figure legend, the reader is referred to the Web version of this article.)
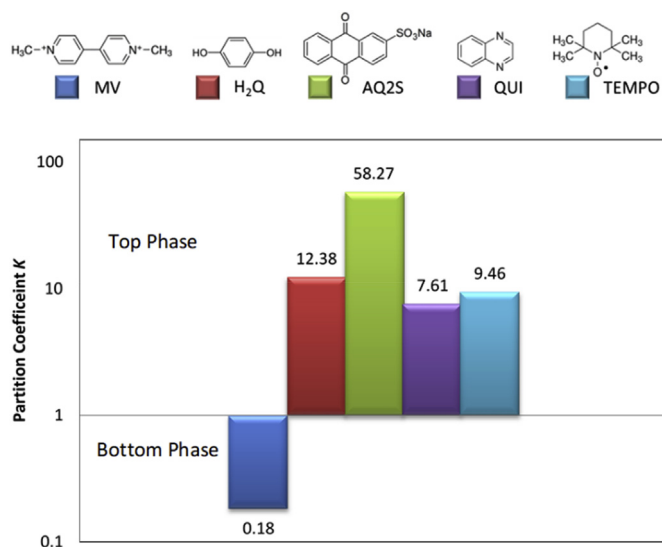
Fig. 2. Partition coefficients of redox organic molecules between the PEG and salt-rich phases in the studied ABS. Chemical structures and abbreviations for the organic redox molecules are also given.

thus preferentially migrates to the bottom phase, which is salt-rich, whereas the rest are more hydrophobic and consequently preferentially migrate to the top PEG-rich phase. With the exception of MV, all molecules exhibit a partition coefficient higher than 7, meaning that their concentration in the top phase is at least 7 times higher than in the bottom phase. Thus, all of them are suitable species in terms of partitioning behavior for being used as active materials in the top phase.

3.1.3. Electrochemical characterization of immiscible phases

As mentioned before, the battery voltage is determined by the difference between the redox potential of the two immiscible phases. Therefore, we investigated the electrochemical properties of the bottom phase containing MV and the four top phases containing QUI, AQ2S, H_2Q, and TEMPO. Cyclic voltammograms (CVs) were performed in a 3-electrode cell and are represented in Fig. S1. The CV of the bottom phase containing MV shows that this molecule undergoes a two steps reduction reaction clearly defined by the appearance of two pairs of redox peaks (Fig. S1a). The first step of the redox reaction at -0.68 V is very reversible and corresponds to the formation of the radical cation. The second step corresponds to the formation of the neutral species at -0.85 V (see mechanism described in Fig. 3). This step shows low reversibility attributed to the stripping process of the neutral species of

MV due to its insolubility [39]. In fact, in most cases, only the first reversible $MV^{2+}/MV^{+\cdot}$ redox reaction is effectively used in RFBs with this molecule. Due to the negative redox potential of MV, the bottom phase is better designed to constitute the anolyte of the battery, whereas the top phase should act as the catholyte.

Among the different candidates for the catholyte (top phase), QUI does not show proper redox activity in this phase (Fig. S1b), whereas AQ2S exhibited quite reversible redox activity but at negative voltages (Fig. S1c); therefore, both were discarded. On the other hand, Fig. S1d and Fig. S1e show that H_2Q and TEMPO exhibit redox activity at positive potential, 0.31 V and 0.55 V, respectively. Accordingly, a battery combining MV in the anolyte with H_2Q in the catholyte will have a theoretical open circuit voltage (OCV) of 1 V whereas the battery combining MV and TEMPO will have an OCV of 1.23 V, as represented in Fig. 3. CV of TEMPO is particularly attractive with two well-defined peaks, corresponding to the reversible redox reaction of TEMPO in which the oxoammonium cation is formed (see TEMPO reaction mechanism in Fig. 3). Therefore, PEG-based ABS containing MV and TEMPO represent a promising approach for developing a Membrane-Free Battery - investigated in more detail as discussed below.

Important physicochemical properties, such as ionic conductivity, pH and density were determined for the investigated PEG-based ABS containing 0.1 M of TEMPO and MV in the initial mixture (Table 1). As expected, the conductivity of the bottom phase is ten times higher than the one obtained for the top phase, due to the higher salt concentration. It is however important to remark that the presence of a salt is necessary in both phases since it will act as a supporting electrolyte providing ionic conductivity and counter-ions during the battery operation. The pH is close to neutrality in the two phases guaranteeing low corrosive and safer electrolytes in comparison with the acidic/alkaline solutions used in conventional aqueous RFB [10,13]. In addition, besides these eco-friendly properties, the use of a polymer-based ABS offers some other advantages such us their low cost and large scale production.

Table 1 also includes the diffusion coefficients (D) and the heterogeneous rate constants (K^0) determined by using Rotating Disk Electrode (RDE) for MV in the bottom (salt-rich) phase and TEMPO in the top (PEG-rich) phase (see Fig. S2). It can be observed that the diffusion of active species is hampered in the top phase with D of TEMPO being one order of magnitude lower than for MV. This can be attributed to the lower salt concentration and lower conductivity of this phase – *cf.* phases compositions given in Fig. 1. However, this difference in conductivity and salt concentration is not a hurdle for having fast charge transfer reactions in both phases, according to the high K^0 values obtained. Thus, the charge transfer resistance at the electrode surface will be low in both catholyte and anolyte anticipating good energy efficiency and power performance in a battery configuration.
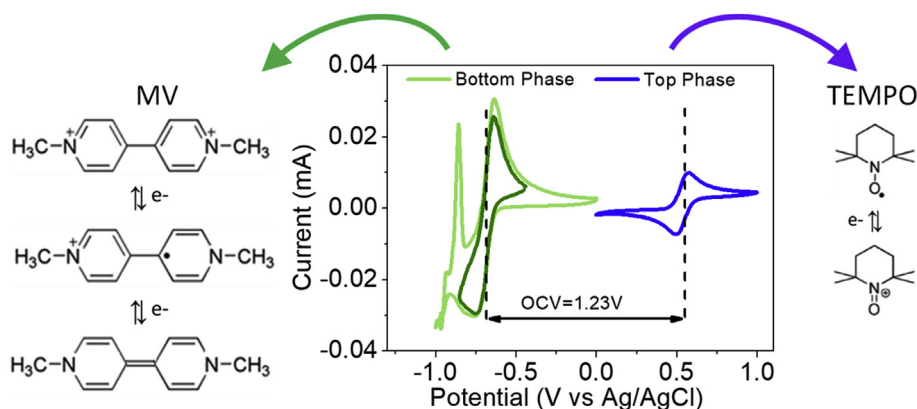

Fig. 3. CV of the immiscible phases of PEG-based ABS containing TEMPO (blue) and MV (light and dark green depending on the voltage limits) at 20 mM concentration. Reaction mechanism of MV and TEMPO. (For interpretation of the references to colour in this figure legend, the reader is referred to the Web version of this article.)

Table 1

Physicochemical properties of each phase of PEG-based ABS containing 0.1 M of TEMPO and MV in the initial mixture. Calculated Diffusion Coefficient (D) and Rate Constant (K^0) for MV and TEMPO in bottom and top phases, respectively.

	Composition (wt%)	Density (g·L^{-1})	pH	Conductivity (mS·cm^{-1})	Diffusion Coefficient (D) (cm^2·s^{-1})	Rate Constant (K^0) (cm·s^{-1})
Top Phase	31.7% PEG 3.2% salt (~0.23 M)	1068	6.28	8.55	$9.09 \cdot 10^{-7}$	$2.53 \cdot 10^{-3}$
Bottom Phase	1.19% PEG 17.75% salt (~1.4 M)	1145	5.04	85.7	$5.01 \cdot 10^{-6}$	$3.41 \cdot 10^{-3}$

3.2. Electrochemical performance of Total Aqueous Membrane-Free Battery

The reliability of ABS application as a Membrane-Free Battery was demonstrated by assembling a full battery just by introducing one carbon felt electrode in each phase. In order to test this new concept of battery in practical conditions, the concentration of active species in the initial mixture was as high as 0.1 M for both TEMPO and MV. The demonstration of the cell was conducted in a static cell in which the same volume of the two phases was added. As illustrated in Fig. 4, the top-phase (TEMPO-rich) constitutes the catholyte and the bottom phase (MV-rich) corresponds to the anolyte of this Membrane-Free Battery. It should be mentioned that this system offers several economic, environmental and safety advantages: i) PEG-based ABS are nontoxic and non-flammable with all components being inexpensive and commercially available in bulk quantities; ii) the two immiscible electrolytes are based on non-corrosive, neutral-pH aqueous solutions; iii) the active species are tunable and commercially available organic molecules; iiv) the battery operates without any separator which reduces significantly the battery cost.

Fig. 4b shows the voltage profile of the full battery, as well as the potential profiles of the individual electrolytes and the interface. The battery voltage exhibits clear and very stable plateaus during charging and discharging at 1.15 V and 1.05 V, respectively, which are very close to the theoretical voltage calculated from the CV (1.23 V, Fig. 3). The individual profiles of the catholyte and anolyte display very small overpotentials and flat and constant plateaus at 0.5 V for the catholyte and −0.6 V for the anolyte, being in good agreement with CV experiments.

The overpotential of the catholyte is higher than for the anolyte probably due to the lower conductivity and diffusion coefficient of the active species in this phase. It should be noticed that the interface overpotential is negligible (only 8.3% of total) establishing a clear advantage of this Membrane-Free configuration compared to conventional RFB in which the membrane overpotential contributes significantly to enhance the battery internal resistance. In fact, the overall resistance of this Membrane-Free Battery is very small which can enhance greatly the voltage efficiency in comparison with conventional RFB.

Fig. 4c and Fig. S3 show the polarization curve of the battery and the evolution of the individual potentials of the two electrolytes and the interface at 20% of state of charge (SOC). As can be seen in Fig. S3, the catholyte suffers from higher polarization than the anolyte during the experiment. As mentioned before, this behavior is due to the lower conductivity and diffusion coefficient shown by the catholyte, which is caused by the higher content of polymer in this phase. The influence of the polymer-rich phase in the battery performance is stronger in charge because of the higher restricted diffusion of the active species to the electrode surface during charging. The polarization response demonstrates a maximum power density output of 23 mW cm^{-2} at 30 mA cm^{-2} (Fig. 4c, orange trace). It is worth to remark that this value of power density is more than 12 times higher than the pioneering example of Membrane-Free Battery [26]. This significant increase can be attributed to the replacement of the ionic liquid anolyte which exhibited low conductivity and high viscosity by an aqueous electrolyte.

Fig. 5a shows the discharge profiles of the battery at different current densities. It should be noticed that considering that the theoretical voltage is 1.23 V, the discharge profile exhibits an ohmic drop as small as
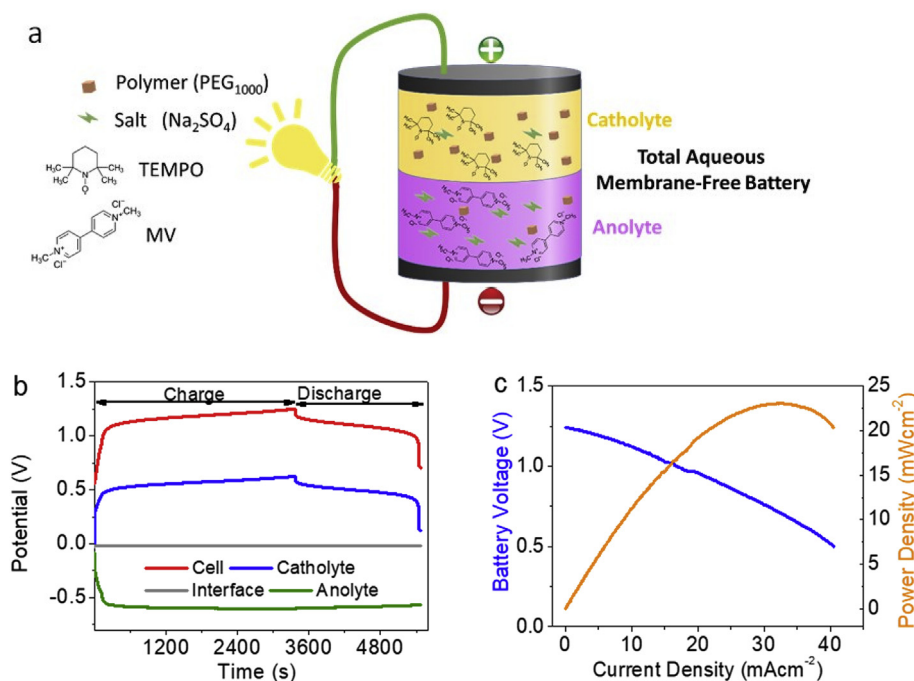

Fig. 4. a) Schematic illustration of the Total Aqueous Membrane-Free Battery, b) Galvanostatic charge-discharge of the battery (20 %SOC) and individual potential profiles of each electrolyte and the interface; charge at C/4 and discharge at C/5. c) Polarization curve of the battery (20 %SOC).
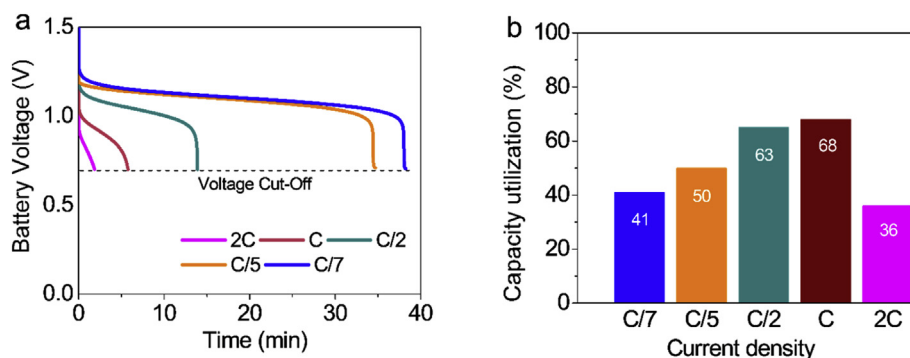
Fig. 5. a) Discharge battery voltage profile at different current densities (20 %SOC). b) Capacity test at different current densities (20 %SOC).

40 mV at C/7 and it increases only up to 330 mV when high current density (2C) is applied. As expected in any type of battery, increasing the current density causes a drop in the discharge voltage motivated by a higher overpotential as a consequence of the diffusion limitations. It is important to remark that even at moderate to high C-rates the battery shows a voltage close to 1 V.

Fig. 5b shows the percentage of capacity utilization, defined as the ratio between the discharge capacity and the theoretical capacity at specific SOC, at different discharge rates. The highest capacity utilization is attained at 1C with a discharge capacity close to the 70% of the theoretical one. Contrarily to typical battery behavior, decreasing the current density leads to lower capacity. This non-conventional trend might be attributed to the self-discharge phenomenon that in this system is due to the direct chemical reaction that leads to a direct electron exchange at the interface (see Fig. S4). This interesting phenomenon that is inherent to the Membrane-Free configuration is also very important for microfluidic membrane-less batteries but, to the best of our knowledge, it has not been investigated in detail. The dimension of the self-discharge depends on the residence time of the active species within the cell and thus becomes more relevant in a static configuration (where the residence time is infinite). However, the residence time of the active species and therefore the self-discharge can be minimized in a flow configuration.

The self-discharge process is based on a chemical reaction between the oxidized species and the reduced species generated during the charge step. Once they are generated, they diffuse up to the interphase and encounter each other, being recombined and coming back to their original state. Consequently, no cross-migration through the interphase of the full reduced/oxidized species will occur which makes possible keep constant the concentration of active molecules in each phase. Although a thorough investigation is out of the scope of this article, the self-discharge was analyzed by monitoring the evolution of the battery open circuit voltage (OCV) over time (starting at 20% SOC). Fig. S4 shows that the initial OCV coincides with the theoretically calculated but it slowly decreases during the experiment (at $1\,\text{mV}\,\text{min}^{-1}$, calculated

from the lineal part of the curve). In fact, after 260 min, the battery was fully discharged due to the abovementioned self-discharge process. As evidenced by the experiments performed at different current densities (Fig. 5), the loss of capacity due to the self-discharge is more relevant in experiments performed at C-rates lower than 1C, since the effective residence time (time needed to discharge completely) is longer. This was demonstrated through experiments in which the discharge current was decreased right after having discharged the battery completely at a certain C. Fig. S5a shows that if the initial discharge was performed at low currents (<1C), the battery was not able to deliver additional capacity in the subsequent discharge at lower currents. This indicates that there are not active species available in the electrolyte, probably due to the direct electron exchange occurring at the interface. On the contrary, if the battery is initially discharged at 2C, in the subsequent discharge at 1C, additional capacity is delivered denoting that there are still active species available in the electrolyte (see Fig. S5b). Therefore, it was demonstrated that the self-discharge becomes irrelevant (contributes < 2% to the discharge) when the effective residence time is short as occurs at 2C where the low capacity utilization (36%) is exclusively attributed to diffusion limitations as in any other battery technology.

An extended charge-discharge experiment was performed to analyze the long-term battery behavior over 550 cycles. The evaluation of the capacity retention over cycles (Fig. 6a) highlights the stable cycling performance of the battery. After 550 cycles the battery exhibited more than 99.99% capacity retention per cycle. The trend of coulombic, voltage and energy efficiencies are displayed in Fig. 6a. The coulombic efficiency remains constant around 82% over the cycling test as well as the voltage efficiency which is one of the highest reported [14–16, 35–37], and ascribed to the fast kinetics and remarkable low overpotentials exhibited by the battery. On account of this, the averaged energy efficiency of the battery is 67% which is comparable and even higher than the one obtained in conventional neutral aqueous RFB [15, 16,37](see Table S2). Compared to our previous work based on an IL-ABS [33], the PEG-based ABS battery reported here is more environmental friendly, less expensive, contains significantly higher
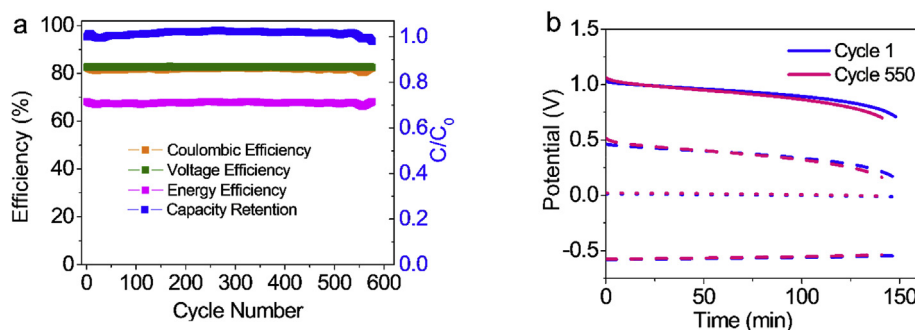

Fig. 6. Cyclability test of the battery (5 %SOC), charging at C/2 and discharging at C. a) Efficiency and capacity retention vs cycle number. b) Individual potential profiles during cycling charged the battery completely at a certain C.

concentration of active species (0.1 M vs. 20 mM), demonstrates a stable performance over longer cycling and exhibit good electrochemical performance (82% CE, 80% VE, 67% EE). The stability was also confirmed by the potential profiles of the individual electrolytes and the interface which remain stable over cycling (Fig. 6b). Likely, the excellent long-term stability of the battery is credited due to the absence of crossover during the battery operation. As mentioned before, the crossover/cross-contamination of the active species in this battery concept was appraised by the determined partition coefficients. Once the equilibrium is established, there is no significant diffusive migration of the active species between the phases through the interface. Thus, the study of partition affinity offers the possibility to control the composition and to avoid the crossover during operation, which guarantees a stable and reliable cycling battery performance.

4. Conclusions

In this work we demonstrate that Aqueous Biphasic Systems can act as a Total Aqueous Membrane-Free Battery, using organic redox compounds with proper redox potentials and suitable partitioning coefficients. Through the study of the partitioning and electrochemical behaviour of several organic active molecules in PEG-based ABS, TEMPO and MV were found to be the most suitable for the catholyte (top phase) and anolyte (bottom phase), respectively. The different composition of the phases/electrolytes demonstrated to have a significant influence on the battery performance since the polymer-rich phase (acting as the catholyte) showed lower conductivity and smaller diffusion coefficient. However, both electrolytes, as well as the interface, displayed low overpotentials during the charge-discharge tests, favourably comparing with conventional RFB where the membrane contributes greatly to increase the internal resistance. The open circuit voltage of the battery coincides with the theoretical one (1.23 V) and the capacity utilization was as high as 68% at high current density (20% SOC). The maximum power density was as high as $23 \, mW \, cm^{-2}$ at $30 \, mA \, cm^{-2}$, being more than 12 times higher than our pioneering example of Membrane-Free Battery. In addition, the battery showed an excellent long-term cycling with a capacity retention 99.9% over 550 cycles and an exceptional round-trip efficiency (70%). This excellent long-term performance of the battery confirms the thermodynamic study of the partition of the active species as a good strategy to avoid the crossover during battery operation. These results highlight the potential of the Membrane-Free Batteries based on ABS as a new energy storage technology by overcoming some technical hurdles of the conventional RFB related to membrane issues, corrosive electrolytes or expensive and limited metallic reactants. Besides the complete removal of the membrane, this battery offers additional advantages since the employed PEG-based ABS is non-expensive, non-corrosive, non-flammable and environmental-friendly. On account of these reasons, this membrane-free battery can be suitable for future applications in non-industrialized areas where contamination with toxic and corrosive vanadium electrolytes can be devastating.

As an inherent aspect of Membrane-Free battery technology, we anticipate that the self-discharge phenomena will be one of the most important challenges that this new technology should address in near future. Some aspects such as cell design, operation conditions and fluidodynamics, and their effect on the battery performance, including self-discharge processes, are currently being investigated in our laboratory.

Declaration of competing interest

The authors declare no competing financial interest.

Acknowledgment

Appendix A. Supplementary data

Parameters A, B and C obtained from Merchuk fitting. Comparison of the present battery with literature reports based on the same active species

CV of different organic compounds partitioning in bottom and top phase of PEG-based ABS.

RDE experiments and fitting of ABS containing TEMPO in top-phase and MV in bottom phase.

Self-discharge experiments.

Supplementary data to this article can be found online at https://doi.org/10.1016/j.ensm.2019.11.011.

References

[1] H. Zhao, Q. Wu, S. Hu, H. Xu, C.N. Rasmussen, Review of energy storage system for wind power integration support, Appl. Energy 137 (2015) 545–553, https://doi.org/10.1016/j.apenergy.2014.04.103.

[2] S. Weitemeyer, D. Kleinhans, T. Vogt, C. Agert, Integration of Renewable Energy Sources in future power systems: the role of storage, Renew. Energy 75 (2015) 14–20, https://doi.org/10.1016/j.renene.2014.09.028.

[3] A. Berrada, K. Loudiyi, Operation, sizing, and economic evaluation of storage for solar and wind power plants, Renew. Sustain. Energy Rev. 59 (2016) 1117–1129, https://doi.org/10.1016/j.rser.2016.01.048.

[4] M. Yekini Suberu, M. Wazir Mustafa, N. Bashir, Energy storage systems for renewable energy power sector integration and mitigation of intermittency, Renew. Sustain. Energy Rev. 35 (2014) 499–514, https://doi.org/10.1016/j.rser.2014.04.009.

[5] P. Alotto, M. Guarnieri, F. Moro, Redox flow batteries for the storage of renewable energy: a review, Renew. Sustain. Energy Rev. 29 (2014) 325–335, https://doi.org/10.1016/j.rser.2013.08.001.

[6] F. Pan, Q. Wang, Redox species of redox flow batteries: a review, Molecules 20 (2015) 20499–24517, https://doi.org/10.3390/molecules201119711.

[7] H. Prifti, A. Parasuraman, S. Winardi, T.M. Lim, M. Skyllas-Kazacos, Membranes for redox flow battery applications, Membranes 2 (2012) 275–306, https://doi.org/10.3390/membranes2020275.

[8] J. Winsberg, T. Hagemann, T. Janoschka, M.D. Hager, U.S. Schubert, Redox-flow batteries: from metals to organic RedoxActive materials, Angew. Chem. Int. Ed. 55 (2016) 2–28, https://doi.org/10.1002/anie.201604925.

[9] W. Wang, V. Sprenkle, Energy storage: redox flow batteries go organic, Nat. Chem. 8 (2016) 204–206, https://doi.org/10.1038/nchem.2466.

[10] B. Yang, L. Hoober-Burkhardt, F. Wang, G.K. Surya Prakash, S.R.J. Narayanan, An inexpensive aqueous flow battery for large-scale electrical energy storage based on water-soluble organic redox couples, Electrochem. Soc. 161 (2014) A1371–A1380, https://doi.org/10.1149/2.1001409jes.

[11] B. Huskinson, M.P. Marshak, C. Suh, S. Er, M.R. Gerhardt, C.J. Galvin, X. Chen, A. Aspuru-Guzik, R.G. Gordon, M.J. Aziz, A metal-free organic–inorganic aqueous flow battery, Nature 505 (2014) 195–198, https://doi.org/10.1038/nature12909.

[12] J. Winsberg, C. Stolze, S. Muench, F. Liedl, M.D. Hager, U.S. Schubert, TEMPO/Phenazine combi-molecule: a redox-active material for symmetric aqueous redox-flow batteries, ACS Energy Lett 1 (2016) 976–980, https://doi.org/10.1021/acsenergylett.6b00413.

[13] K. Lin, Q. Chen, M.R. Gerhardt, L. Tong, S.B. Kim, L. Eisenach, A.W. Valle, D. Hardee, R.G. Gordon, M.J. Aziz, M.P. Marshak, Alkaline quinone flow battery, Science 349 (2015) 1529–1532, https://doi.org/10.1126/science.aab3033.

[14] T. Liu, X. Wei, Z. Nie, V. Sprenkle, W. Wang, A total organic aqueous redox flow battery employing a low cost and sustainable Methyl viologen anolyte and 4-HO-TEMPO catholyte, Adv. Energy Mater. 6 (2016) 1501449, https://doi.org/10.1002/aenm.201501449.

[15] T. Janoschka, N. Martin, M.D. Hager, U.S. Schubert, An aqueous redox-flow battery with high capacity and power: the TEMPTMA/MV system, Angew. Chem. Int. Ed. 55 (2016) 14427–14430, https://doi.org/10.1002/anie.201606472.

[16] B. Hu, C. Debruler, Z. Rhodes, T. Liu, Long-cycling aqueous organic redox flow battery (AORFB) toward sustainable and safe energy storage, J. Am. Chem. Soc. 139 (2017) 1207–1214, https://doi.org/10.1021/jacs.6b10984.

[17] F.R. Brushett, J.T. Vaughey, A.N. Jansen, An all-organic non-aqueous lithium-ion redox flow battery, Adv. Energy Mater. 2 (2012) 1390–1396, https://doi.org/10.1002/aenm.201200322.

[18] Z. Li, S. Li, S. Liu, K. Huang, D. Fang, F. Wang, S. Peng, Electrochemical properties of an all-organic redox flow battery using 2,2,6,6-tetramethyl-1-piperidinyloxy and N-methylphthalimide, Electrochem. Solid State Lett. 14 (2011) A171–A173, https://doi.org/10.1149/2.012112esl.

[19] S.K. Park, J. Shim, J. Yang, K.H. Shin, C.S. Jin, B.S. Lee, Y.S. Lee, J.D. Jeon, Electrochemical properties of a non-aqueous redox battery with all-organic redox couples, Electrochem. Commun. 59 (2015) 68–71, https://doi.org/10.1016/j.elecom.2015.07.013.

[20] X. Wei, W. Duan, J. Huang, L. Zhang, B. Li, D. Reed, W. Xu, V. Sprenkle, W. Wang, A high-current, stable nonaqueous organic redox flow battery, ACS Energy Lett 1 (2016) 705–711, https://doi.org/10.1021/acsenergylett.6b00255.

[21] X. Wei, W. Xu, J. Huang, L. Zhang, E. Walter, C. Lawrence, M. Vijayakumar, W.A. Henderson, T. Liu, L. Cosimbescu, B. Li, V. Sprenkle, W. Wang, Radical compatibility with nonaqueous electrolytes and its impact on an all-organic redox flow battery, Angew. Chem. Int. Ed. 54 (2015) 8684–8687, https://doi.org/10.1002/anie.201501443.

[22] A.P. Kaur, N.E. Holubowitch, S. Ergun, C.F. Elliott, S.A. Odom, A highly soluble organic catholyte for non-aqueous redox flow batteries, Energy Technol. 3 (2015) 476–480, https://doi.org/10.1002/ente.201500020.

[23] B. Schwenzer, J. Zhang, S. Kim, L. Li, J. Liu, Z. Yang, Membrane development for vanadium redox flow batteries, ChemSusChem 4 (2011) 1388–1406, https://doi.org/10.1002/cssc.201100068.

[24] S.-H. Shin, S.-H. Yun, S.-H. Moon, A review of current developments in non-aqueous redox flow batteries: characterization of their membranes for design perspective, RSC Adv. 3 (2013) 9095–9116, https://doi.org/10.1039/C3RA00115F.

[25] M.O. Bamgbopa, S. Almheiri, H. Sun, Prospects of recently developed membraneless cell designs for redox flow batteries, Renew. Sustain. Energy Rev. 70 (2017) 506–518, https://doi.org/10.1016/j.rser.2016.11.234.

[26] P. Navalpotro, J. Palma, M. Anderson, R. Marcilla, A membrane-free redox flow battery with two immiscible redox electrolytes, Angew. Chem. Int. Ed. 56 (2017) 12460–12465, https://doi.org/10.1002/anie.201704318.

[27] P. Navalpotro, N. Sierra, C. Trujillo, I. Montes, J. Palma, R. Marcilla, Exploring the versatility of membrane-free battery concept using different combinations of immiscible redox electrolytes, ACS Appl. Mater. Interfaces 10 (2018) 41246–41256, https://doi.org/10.1021/acsami.8b11581.

[28] K. Gong, F. Xu, M.G. Lehrich, X. Ma, S. Gu, Y.J. Yan, Exploiting immiscible aqueous-nonaqueous electrolyte interface toward a membraneless redox-flow battery concept, Electrochem. or. Soc. 164 (2017) A2590–A2593, https://doi.org/10.1149/2.1241712jes.

[29] M.O. Bamgbopa, Y. Shao-Horn, R. Hashaikeh, S. Almheiri, Cyclable membraneless redox flow batteries based on immiscible liquid electrolytes: demonstration with all-iron redox chemistry, Electrochim. Acta 267 (2018) 41–50, https://doi.org/10.1016/j.electacta.2018.02.063.

[30] S. Bamberger, E.D. Brooks, K.A. Sharp, J.M.V. Alstine, T.J. Webber, in: H. Walter, E.D. Brooks, D. Fischer (Eds.), Partitioning in Aqueous Two-phase Systems Theory, Methods, Uses and Applications to Biotechnology, Academic Press, INC, London, 1985.

[31] B.Y. Zaslavsky, Aqueous Two-phase Partitioning Physical Chemistry and Bioanalytical Applications, Marcel Dekker, INC, New York, 1995.

[32] M.G. Freire, A.F.M. Cláudio, J.M.M. Araújo, J.A.P. Coutinho, I.M. Marrucho, J.N.C. Lopes, L.P.N. Rebelo, Aqueous biphasic systems: a boost brought about by using ionic liquids, Chem. Soc. Rev. 41 (2012) 4966–4995, https://doi.org/10.1039/C2CS35151J.

[33] P. Navalpotro, C.M.S.S. Neves, J. Palma, M.G. Freire, J.A.P. Coutinho, R. Marcilla, Pioneering use of ionic liquid-based aqueous biphasic systems as membrane-free batteries, Adv. Sci. 1800576 (2018), https://doi.org/10.1002/advs.201800576.

[34] J. Winsberg, C. Stolze, A.M. Schwenke, S. Muench, M.D. Hager, U.S. Schubert, Aqueous 2,2,6,6-tetramethylpiperidine-N-oxyl catholytes for a high-capacity and high current density oxygen-insensitive hybrid-flow battery, ACS Energy Lett 2 (2017) 411–416, https://doi.org/10.1021/acsenergylett.6b00655.

[35] B. Hu, C. Seefeldt, C. DeBruler, T.L. Liu, Boosting the energy efficiency and power performance of neutral aqueous organic redox flow batteries, J. Mater. Chem. A 5 (2017) 22137–22145, https://doi.org/10.1039/C7TA06573F.

[36] J. Luo, B. Hu, C. Debruler, T.L. Liu, A π-conjugation extended viologen as a two-electron storage anolyte for total organic aqueous redox flow batteries, Angew. Chem. Int. Ed. 57 (2018) 231–235, https://doi.org/10.1002/anie.201710517.

[37] E.S. Beh, D. De Porcellinis, R.L. Gracia, K.T. Xia, R.G. Gordon, M.J. Aziz, A neutral pH aqueous organic–organometallic redox flow battery with extremely high capacity retention, ACS Energy Lett 2 (2017) 639–644, https://doi.org/10.1021/acsenergylett.7b00019.

[38] J.C. Merchuk, B.A. Andrews, J.A.J. Asenjo, Aqueous two-phase systems for protein separation. Studies on phase inversion, Chromatogr. B Biomed. Sci. Appl. 711 (1998) 285–293, https://doi.org/10.1016/S0378-4347(97)00594-X.

[39] C.L. Bird, A.T. Kuhn, Electrochemistry of the viologens, Chem. Soc. Rev. 10 (1981) 49–82, https://doi.org/10.1039/CS9811000049.